NJC

Accepted Manuscript

This is an *Accepted Manuscript*, which has been through the Royal Society of Chemistry peer review process and has been accepted for publication.

Accepted Manuscripts are published online shortly after acceptance, before technical editing, formatting and proof reading. Using this free service, authors can make their results available to the community, in citable form, before we publish the edited article. We will replace this *Accepted Manuscript* with the edited and formatted *Advance Article* as soon as it is available.

You can find more information about *Accepted Manuscripts* in the Information for Authors.

Please note that technical editing may introduce minor changes to the text and/or graphics, which may alter content. The journal's standard Terms & Conditions and the Ethical guidelines still apply. In no event shall the Royal Society of Chemistry be held responsible for any errors or omissions in this *Accepted Manuscript* or any consequences arising from the use of any information it contains.

ROYAL SOCIETY OF CHEMISTRY

www.rsc.org/njc

Aggregate-based sub-CMC Solubilization of *n*-Alkanes by Monorhamnolipid Biosurfactant

Hua Zhong[1,2,3*], Xin Yang[1,2], Fei Tan[1,2], Mark L Brusseau[3], Lei Yang[1,2], Zhifeng Liu[1,2], Guangming Zeng[1,2], Xingzhong Yuan[1,2]

[1] College of Environmental Science and Engineering, Hunan University, Changsha 410082, China;

[2] Key Laboratory of Environmental Biology and Pollution Control (Hunan University), Ministry of Education, Changsha, 410082, China;

[3] Department of Soil, Water and Environmental Science, University of Arizona, Tucson, Arizona 85721, USA;

Submitted to:

New Journal of Chemistry

Revised on 16 November 2015

[*] Corresponding author at: Department of Soil, Water and Environmental Science, University of Arizona, 1177 E 4th St., Tucson, AZ 85721, U.S.A. Tel.: +01-520-626-4191; E-mail address: zhonghua@hnu.edu.cn; zhonghua@email.arizona.edu (H. Zhong).

Email Addresses:

Hua Zhong: zhonghua@email.arizona.edu

Xin Yang: yx2013@hnu.edu.cn

Fei Tan: tanfei_2013@163.com

Mark L. Brusseau: brusseau@email.arizona.edu

Lei Yang: wlwyanglei@126.com

Zhifeng Liu: lzf18182002@163.com

Guangming Zeng: zgming@hnu.edu.cn

Xingzhong Yuan: yxz@hnu.edu.cn

Abstract

Solubilization of *n*-decane, dodecane, tetradecane and hexadecane by monorhamnolipid biosurfactant (monoRL) at concentrations near the critical micelle concentration (CMC) was investigated. The apparent solubility of all the four alkanes increases linearly with increasing monoRL concentration either below or above CMC. The capacity of solubilization presented by the molar solubilization ratio (MSR), however, is stronger at monoRL concentrations below CMC than above CMC. The MSR decreases following the order dodecane > decane > tetradecane > hexadecane at monoRL concentration below CMC. Formation of aggregates at sub-CMC monoRL concentrations was demonstrated by dynamic light scattering (DLS) and cryo-transmission electron microscopy examination. DLS-based size (d) and zeta potential of the aggregates decrease with increasing monoRL concentration. The surface excess (Γ) of monoRL calculated based on alkane solubility and aggregate size data increases rapidly with increasing bulk monoRL concentration, and then asymptotically approaches the maximum surface excess (Γ_{max}). Relation between Γ and d indicates that the excess of monoRL molecules at the aggregate surface greatly impacts the surface curvature. The results demonstrate formation of aggregates for alkane solubilization at monoRL concentrations below CMC, indicating the potential of employing low-concentration rhamnolipid for enhanced solubilization of hydrophobic organic compounds.

Keywords: biosurfactant, monorhamnolipid, *n*-alkane, critical micelle concentration,

solubilization, aggregation

1. Introduction

Biosurfactants are amphiphilic molecules produced by microbes. They have the properties of typical surfactants, such as lowering interfacial tension, wetting surface, foaming, and causing solubilization or emulsification of hydrophobic organic compounds (HOCs). Due to their advantages over synthetic surfactants, e.g. low toxicity,[1] high degradability and environmental compatibility,[1] and high efficiency,[2,3] biosurfactants have received increased use for many applications in areas such as chemical manufacturing, pharmaceuticals, contamination remediation, etc.[4] Solubilization of organic compounds is one of the key functions for these applications of biosurfactants. For example, biosurfactant-enhanced aquifer remediation for removal of nonaqueous-phase-liquid HOCs is primarily based on the mechanism of solubilization.[5, 6]

Solubilization of HOCs by surfactants has been studied extensively at high surfactant concentrations, i.e. higher than critical micelle concentration (CMC).[7-14] Micelles are considered to be of spherical shape with three zones for solubilization: the core, the corona, and the core-corona interface.[15, 16] It is typically assumed that solubilization enhancement of hydrophobic compounds only occurs at surfactant concentrations higher than CMC.[11, 16, 17]

The results of some studies, however, showed that surfactants also solubilize

HOCs at sub-CMC concentrations. For example, result of our prior study showed that synthetic surfactants SDBS and Triton X-100 enhanced solubilization of hexadecane at concentrations below CMC based on an aggregate formation mechanism.[18] There is evidence of similar behavior for biosurfactants, with Zhang and Miller reporting that solubility of octadecane was enhanced by rhamnolipid biosurfactant at sub-CMC concentrations. It is interesting to note that the enhancement was much more significant at concentrations below the CMC than at concentrations above CMC.[8] It was assumed that this sub-CMC enhancement of octadecane solubilization was due to the decrease of water-octadecane interfacial tension.[8] In our prior study of hexadecane solubilization by rhamnolipids, similar results were also observed.[19] Research is needed to delineate the mechanisms contributing to the sub-CMC solubilization capability observed for biosurfactants. This information is also relevant for commercial application of biosurfactants in terms of cost effectiveness.

To date rhamnolipid is the most extensively studied biosurfactant and has the greatest application potential. Solubilization of *n*-alkanes by rhamnolipid at concentrations near CMC was investigated in this study, with a focus on solubilization behavior at concentrations lower than CMC. Monorhamnolipid (monoRL), a group of rhamnolipid species with one rhamnose ring and two alkyl chains (Figure 1), was used in this study. MonoRL is selected because it is the class of species that always exists in rhamnolipid mixture and is the precursor for biosynthesis of dirhamnolipid. Results of our prior study also showed that it appears to have stronger ability over

dirhamnolipid and synthetic surfactants to enhance HOC solubilization at low concentrations.[3,18] It is considered an anionic surfactant under the experiment conditions in this study due to the carboxyl group in the molecule (pK_a=5.6 under ambient temperature [20]). Four linear alkanes (i.e. *n*-decane, *n*-dodecane, *n*-tetradecane and *n*-hexadecane) with different chain lengths were selected to represent HOCs. In addition to *n*-alkanes solubility, characterizations of alkane-monoRL aggregates, such as measurement of aggregate size and zeta potential and cryo-TEM-based observation of aggregate morphology, were implemented. Finally, surfactant interface partition theory, an assumption of spherical aggregates, and surfactant mass balance was used to interpret the sub-CMC solubilization of the alkanes by the rhamnolipid.

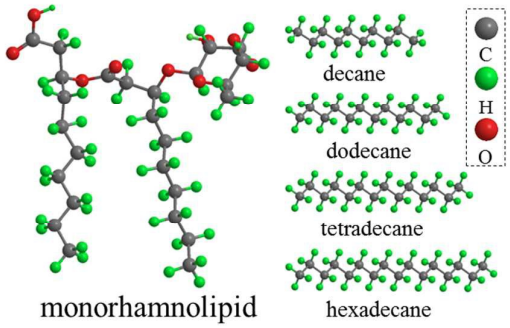

Figure 1 Molecular structure of monoRL and the four *n*-alkanes.

2. Theoretical Background

Based on the classical model regarding the structure of alkane-surfactant aggregates formed in solution for alkane solubilization, the aggregates are assumed to be spherical, comprising the alkane residing in the core zone and a layer of surfactant molecules on surface with their alkyl chains intermingling in the core with the alkane

molecules. Rhamnolipid molecules reside in bulk solution or as the outer layer of the aggregates, for which the partition can be described using Gibbs and Langmuir adsorption equations [21-23]. In addition, the total mass of rhamnolipid in bulk solution and as aggregates is equal to the mass of rhamnolipid initially added. Based on these assumptions, partition of rhamnolipid between bulk solution and aggregate phase at solubilization equilibrium can be calculated using measures of interfacial tension and aggregate size. The theoretical details can be found in ref. 18.

3. Materials and Methods

3.1 Materials

The monoRL biosurfactant (purity > 99.9%) was purchased from Zijin Biological Technology Co., Ltd. (Huzhou, China). Constituent characterization of the monoRL is described by Zhong et al.[24]. The monoRL comprises five species of Rha-C_{10}-C_8, Rha-C_{10}-$C_{10:1}$, Rha-C_{10}-C_{10}, Rha-C_{10}-$C_{12:1}$ and Rha-C_{10}-C_{12}, where the abbreviation Rha-C_x-$C_{y:z}$ represents the individual component with x and y as the carbon atom number of each alkyl chain in the lipid moieties, and z as the number of unsaturated bonds in lipid moieties. Rha-C_{10}-C_{10} at the relative molar abundance of 75.5% is the major component.

The *n*-alkanes (*n*-decane, *n*-dodecane, *n*-tetradecane and *n*-hexadecane) (purity > 99%) were purchased from Sigma-Aldrich (St. Louis, Mo., U.S.). The selected properties of the *n*-alkanes are listed in Table 1 and molecule structure is shown in

Figure 1. *n*-Octane (purity > 95.0%) and HPLC grade ethanol were purchased from Damao Chemical Reagent Co. Ltd. (Tianjin, China). All other chemicals were of analytical grade and used as received. Ultra-pure water with electrical resistivity of 18.2 MΩ·cm produced by UPT-Ⅱ-40 (Ulupure, Chengdu, China) was used throughout the experiment. Phosphate buffer (PBS, 1.24 g/L KH_2PO_4 and 1.35 g/L $K_2HPO_4 \cdot 3H_2O$, pH 6.8) was used as the background electrolyte solution for monoRL solubilization. It provides a stable concentration of counterions, which is important for application of the Gibbs adsorption equation for monoRL with ionic nature. In this PBS buffer, the degree of dissociation for the monoRL is 94% based on pK_a of 5.6 [20]. Such a high degree of dissociation also supports the assumption that the monoRL is anionic and resides only in bulk solution or at interface in this study.

Table 1. Selected properties of *n*-alkanes and the alkane-PBS interfacial partitioning coefficients for monoRL

n-Alkane	Formula	Molecule weight (g/mol)	Water solubility [a] (μM, 25°C)	log K_{ow} [b] (25°C)	Density [c] (g/cm^3, 25°C)	CMC[d] (μM)	K (m^3/mol)	Γ_{max} (mol/m^2)	A_m (nm^2)
decane	$C_{10}H_{22}$	142	0.37	5.01	0.73	150	0.98×10^3	3.1×10^{-6}	0.54
dodecane	$C_{12}H_{26}$	170	0.02	6.10	0.75	155	1.81×10^3	2.9×10^{-6}	0.58
tetradecane	$C_{14}H_{30}$	198	0.01	7.20	0.76	169	0.74×10^3	3.6×10^{-6}	0.46
hexadecane	$C_{16}H_{34}$	226	0.0004	8.25	0.77	152	0.57×10^3	4.1×10^{-6}	0.41

[a] Solubilities of *n*-alkanes are reported by NCBI (ref. 25-28)
[b] Octanol-water partition coefficient (K_{ow}) values of *n*-alkanes from NCBI (ref. 25-28)
[c] Relative density (water=1) of *n*-alkanes from NCBI (ref. 25-28)
[d] Critical micelle concentration (CMC) for monoRL biosurfactant in the presence of *n*-alkanes obtained by *n*-alkane/PBS interfacial tension measurement (CMC obtained by surface tension measurement in the absence of *n*-alkanes is 166 μM)

3.2 Surface and interfacial tension measurement

Interfacial tension between alkane and monoRL solutions with designated monoRL concentrations was measured at 30°C with a tensiometer (JZ-200A, Chengde, China) using the Du Noüy Ring method.[29] In brief, 15 mL of monoRL solution in PBS was prepared in a 50 mL glass beaker. 15 mL of alkane was then carefully added to the top of the monoRL solutions without disturbing the solution. Before the interfacial tension was measured, the beaker was kept at 30°C for half an hour to allow partitioning of monoRL to the water-alkane interface to reach equilibrium. The measurements were reproducible, with the difference of duplicate measurements within ±0.2 mN/m. For reference purposes, the surface tension (interfacial tension between air and solution) of the monoRL solution was also measured.

3.3 Solubilization of *n*-alkane by monoRL

For each *n*-alkane-monoRL combination, 50 μL of alkane was pipetted and spread on the bottom of a 25-mL glass flask. 10 mL of monoRL solution in PBS was then added to the flask and incubated on a reciprocal shaker at 30°C, 120 rpm for 24 h to allow the solubilization to reach equilibrium (result of a preliminary test showed that alkane solubility did not change after 24 h). The flasks were allowed to stand for 2 h for phases to separate, then 4 ml of aqueous solution saturated with only pseudo-solubilized hexadecane was separated using the method described by Zhong et al.[19] 1 mL of the collected samples was removed for alkane concentration

measurement, and another 2 mL was used for measurement of size and zeta potential of the aggregates. The alkane concentration was measured using gas chromatography (Agilent GC 6890N) following the procedures described by Zhong et al.[19]. A control containing 10 mL monoRL solution and no alkane was used to quantify loss of monoRL due to adsorption to the inner wall of the flasks.

The size and zeta potential of aggregate particles were measured using a ZEN3600 Zetasizer Nano (Malvern Instruments, U.K.). The particle size was determined based on the method of dynamic light scattering (DLS) at 633 nm with He-Ne laser working on a 4 mV power. 1 mL of sample was loaded to the DTS-0012 cell and maintained at 30°C. The scattered light was collected by receptor at angle of 173° from light path. The size of the aggregates was expressed in terms of hydrodynamic diameter, which was calculated by using the software associated with the instrument. To obtain the zeta potential of the aggregates, approximately 1 mL of sample was loaded to the DTS1060 folded capillary cell and the electrophoretic mobility of the aggregate particles was measured at 30°C under automatic voltage using laser Doppler velocimetry with M3-PALS technique to avoid electroosmosis. The measured data was converted into corresponding zeta potential applying the Helmholtz-Smoluchowski equation.[30]

3.4 Cryo-Transmission Electron Microscopy (cryo-TEM) observation of hexadecane-monoRL aggregates

A 4 μL drop of solubilized hexadecane solution was placed on a copper grid, and then sent to a FEI Vitrobot sample plunger. The excess sample was removed with filter paper. The grid was then immediately plunged into a bath of liquid ethane and transferred to a bath of liquid nitrogen. The samples were stored in a GATAN model cryo-transfer unit in liquid nitrogen. The morphology of surfactant-hexadecane aggregates was viewed with a Tecnai F20 cryo-transmission electron microscope (FEI, Hillsboro, Oregon) at 120 kV.

4. Results and discussion

4.1 CMC and interfacial partitioning parameters

The dependence of air-PBS and *n*-alkane/PBS interfacial tension on monoRL concentration is presented in Fig. 2a. CMCs calculated using the method described by Zhong et al.[31] are presented in Table 1. The CMCs of monoRL obtained using surface tension or interfacial tension measurements are similar to each other, showing that the non-aqueous phase (air or alkanes) has little impact on CMC. An average CMC of 158±9 μM is obtained.

The interfacial tension data at sub-CMC monoRL concentration are well fitted by equation (3) in ref.18 (Fig. 2b). The Langmuir adsorption constant (K), maximum interfacial access (Γ_{max}), and minimum area per molecule (A_m) obtained for the adsorption are summarized in Table 1. K decreases following the order dodecane > decane > tetradecane > hexadecane. Alkyl chain length of the monoRL is similar to

that of dodecane and decane (Figure 1), which may be favorable for hydrophobic interaction between monoRL and alkane molecules at the interface and hence lower Gibbs energy, resulting in a stronger partitioning of monoRL at the interface for dodecane and decane. However, Γ_{max} is larger (A_m is smaller) for tetradecane and hexadecane, showing that when the adsorption is saturated the monoRL molecules are more compacted at the interface for long-chain alkanes.

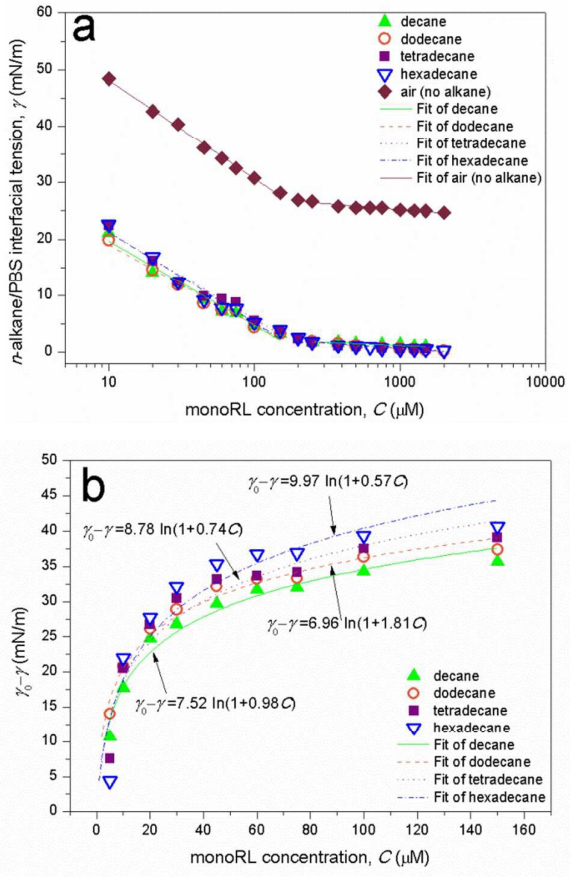

Figure 2 (a) The air-PBS and *n*-alkanes/PBS interfacial tension as a function of monoRL concentration. (b) Interfacial tension-concentration relation regression at monoRL concentrations below CMC using Szyszkowski equation (Equation (3) in ref.18).

225

226 **4.2 Solubilization of *n*-alkanes by monoRL**

227 Apparent solubility of alkanes as a function of total monoRL concentration, C_0,
228 is shown in Fig. 3. For all four alkanes, the solubility is enhanced at monoRL
229 concentrations below CMC. The apparent solubility of each alkane increased linearly
230 with monoRL concentration at different rates below and above CMC.

231 The solubilization capacity of a surfactant for a HOC is presented by the molar
232 solubilization ratio (MSR), which is defined as the increase of solubilized HOC
233 concentration (mol/L) per unit increase of surfactant concentration (mol/L) in the
234 solution, or the slope of the linear solubilization curve.[32] The MSR for the four
235 alkanes are listed in Table 2. MSR for all of the four alkanes are significantly higher at
236 monoRL concentration below CMC than above CMC. Similar results were observed
237 for octadecane solubilization by monoRL,[8] and hexadecane solubilization by SDBS
238 (also an anionic surfactant)[18].

239 These observations indicate a difference in modes of alkane solubilization below
240 and above CMC. The MSR decreases following the order dodecane > decane >
241 tetradecane > hexadecane at monoRL concentrations below CMC (Table 2), which is
242 the same as the order for *K*. This indicates a relationship between alkane
243 solubilization and interfacial partitioning of monoRL. It is worth noting that the MSR
244 for hexadecane solubilization by the monoRL at sub-CMC concentrations (2.55) is
245 larger than that for SDBS (0.84) and Triton X-100 (1.90)[18], indicating higher

solubilization efficiency of biosurfactant monoRL over synthetic surfactants. This is probably due to the presence of the double alkyl chains in the monoRL molecule.

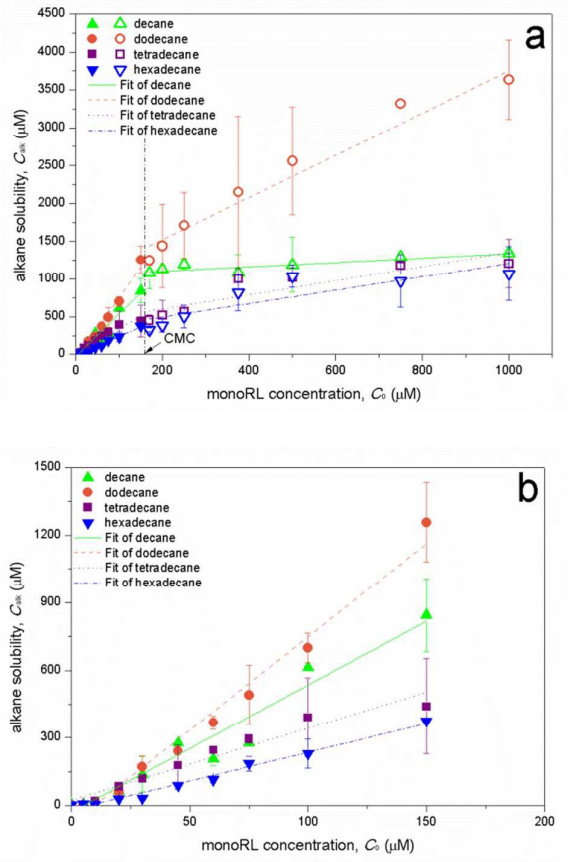

Figure 3 (a) Apparent *n*-alkanes solubility (C_{alk}) versus monoRL total concentration (C_0). Two sets of regressions represent data for below and above the CMC. (b) Zoom-in for C_{alk}-C_0 relation for C_0 lower than CMC. Error bars show mean ± standard deviation.

Table 2. The molar solubilization ratio (MSR) for alkane solubilization by monoRL

n-Alkane	MSR	
	Below CMC	Above CMC

decane	5.73	0.29
dodecane	8.28	2.91
tetradecane	3.27	0.94
hexadecane	2.55	0.89

258

259 **4.3 Size and zeta potential of aggregates**

260 The formation of aggregates was detected by aggregate size measurement using
261 the DLS method. A single peak is observed for the number-based particle size
262 distribution profile, indicating formation of one consistent size of aggregate (Fig.4).
263 The aggregates are observed directly with cryo-TEM, and the spherical aggregate
264 morphology is confirmed (Fig. 5). Also, the size of the aggregates as measured by
265 cryo-TEM is similar to the DLS-measured size. The aggregates shown by cryo-TEM
266 do not appear when hexadecane is equilibrated with aqueous solution without
267 monoRL (data not shown).

268 For all four alkanes, the DLS particle size first decreases rapidly with increase of
269 C_0, and then stabilizes with increase of C_0 to above CMC (Fig. 6). By comparing
270 between alkanes, it is observed that the aggregates size at monoRL concentration of
271 CMC decreases following the order decane ≈ dodecane > tetradecane > hexadecane.
272 This order is in contrast to the order of Γ_{max} for these four alkanes, which is decane ≈
273 dodecane < tetradecane < hexadecane (Table 1).

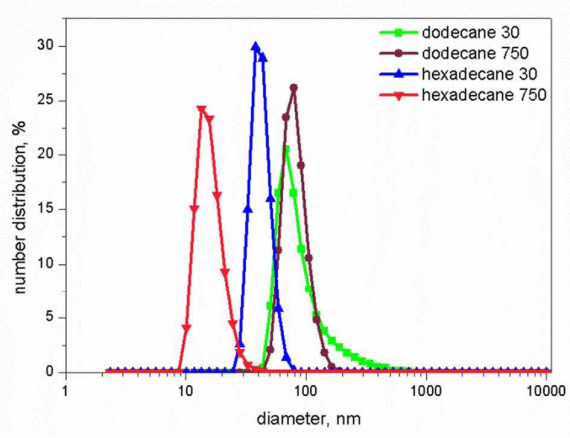

Figure 4 Number distribution of aggregate particles for solubilization of dodecane and hexadecane by monoRL at concentration of 30 μM and 750 μM.

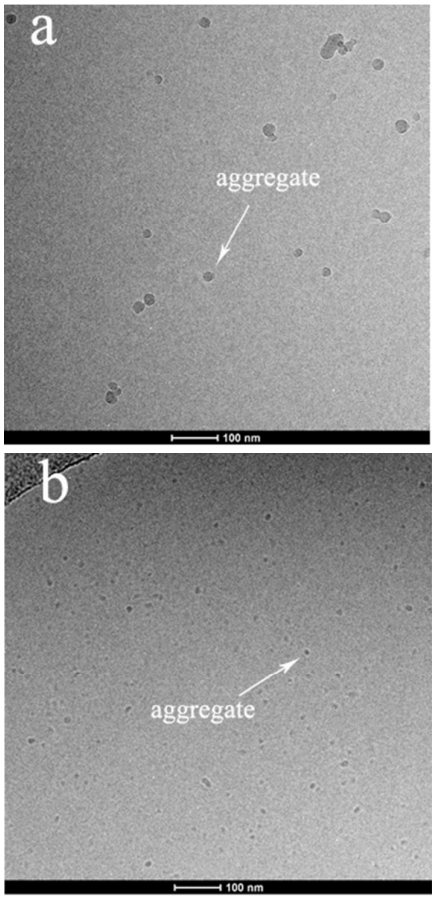

Figure 5 Cryogenic-transmission electron microscopy (cryo-TEM) images showing aggregates for the solubilization of hexadecane by monoRL at monoRL concentration of 30μM (below CMC) (a) and 750μM (above CMC) (b).

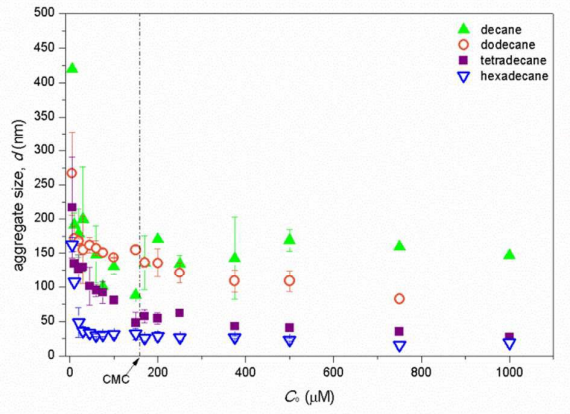

Figure 6 DLS aggregate size (diameter, d) versus the total monoRL concentration (C_0) for the *n*-alkanes solubilization. Error bars show mean ± standard deviation.

Zeta potentials of the aggregates are shown in Fig. 7. The aggregates are negatively charged. The change of zeta potential with increase of C_0 exhibits a similar trend for all four alkanes. It decreases rapidly with increase of C_0 to CMC, and then stabilizes or decreases slowly with further increase of monoRL concentration.

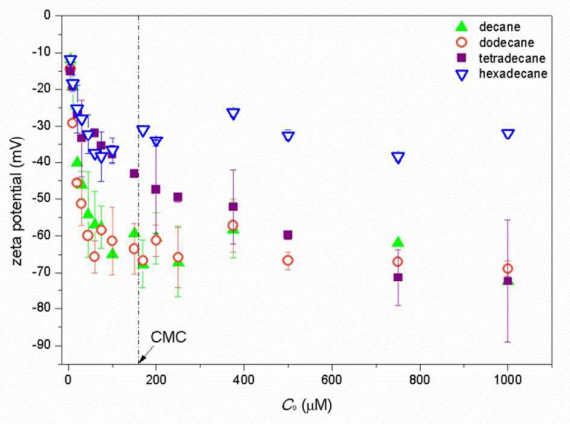

Figure 7 Zeta potential of aggregates versus the monoRL total concentration (C_0) for the *n*-alkanes solubilization. Error bars show mean ± standard deviation.

294 **4.4 Partitioning of monoRL and its relation with aggregation**

295 No emulsion of alkanes in the presence of monoRL was observed in the
296 experiments. Adsorption of the monoRL to the inner wall of the flask was minimal
297 (data not shown). Because very limited volume of alkanes (50 μL, see Materials and
298 Methods section) was used, partition of monoRL to the alkane phase, or to the
299 interface between the floating mass of alkane and the aqueous phase (less than 1 cm^2
300 in contrast to the magnitude of $10 \sim 10^3$ cm^2 for the total surface area of the aggregates
301 according to calculation below), was minimal. Therefore, the monoRL can be
302 assumed to reside either in bulk aqueous solution or in the aggregates. Due to the
303 extremely low water solubility and high octanol-water partition coefficient (K_{ow}) of
304 these four alkanes (Table 1), the amount of freely-dissolved alkane in bulk aqueous
305 phase is minimal and all the solubilized alkane is assumed to be associated with the
306 aggregates. Hence, based on the spherical aggregate assumption, the aggregate
307 surface excess, Γ, and the bulk concentration, C_w, of monoRL monomer were
308 calculated by applying equation (2) and (5) in ref.18 using Γ_{max} and K previously
309 obtained.

310 For all four alkanes, a linear relationship between the apparent solubility of
311 alkane, C_{alk}, and C_w is observed with increase of C_w to CMC (Fig. 8a). This is similar
312 to the relationship between C_{alk} and C_0 (the total monoRL concentration in solution)
313 (Fig. 3). By comparing the slopes of the C_{alk}-C_0 profiles at C_0 below CMC with those
314 of the C_{alk}-C_w profiles (5.7 versus 7.5 for decane, 8.3 versus 10.8 for dodecane, 3.3

versus 5.3 for tetradecane, and 2.55 versus 6.3 for hexadecane), the percentage of the aggregate-associated monoRL is calculated to be 24%, 23%, 38%, and 59% of the total for decane, dodecane, tetradecane, and hexadecane, respectively. Note that the aggregate size for hexadecane is significantly smaller than that for the other three alkanes at C_0 lower than CMC. The higher surface area for smaller particles is responsible for the enhanced partition of monoRL to the aggregates, in spite of the fact that the K and C_{alk} for hexadecane is the smallest among the four alkanes.

The dependence of monoRL surface excess (Γ) and molecule area (A) versus C_w are presented in Fig. 8b. A rapid increase of Γ and decrease of A with increasing C_w are observed when C_w is low. Further increase of C_w causes asymptotic approach of Γ and A to Γ_{max} and A_m, respectively. More significant change of Γ and A is observed for the long-chain alkanes (tetradecane and hexadecane). Based on equation (2) in ref.18, Γ is more sensitive to change of C_w with a smaller K. The K for four alkanes follows the order dodecane > decane > tetradecane > hexadecane (Table 1). Thus, the most significant change of Γ and A over the broadest range of C_w occurred for hexadecane.

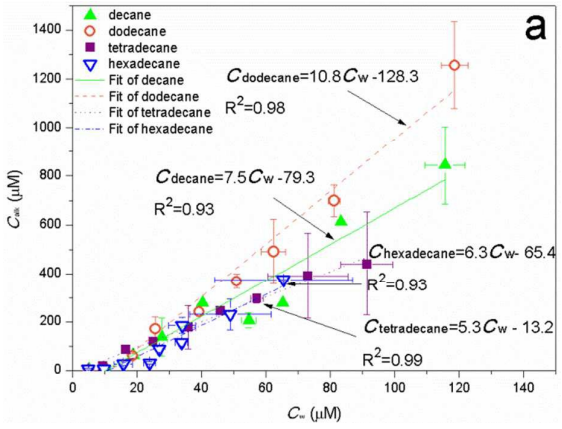

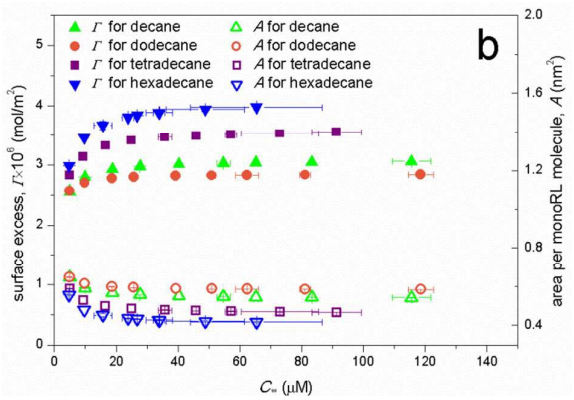

Figure 8 (a) Apparent solubility of *n*-alkanes (C_{alk}) versus the monoRL bulk concentration (C_w) at C_w below CMC. (b) Surface excess (Γ) and molecule area (A) of monoRL on the aggregates surface versus monoRL bulk concentration (C_w). Error bars show mean ± standard deviation.

As shown in Fig. 9, for all four alkanes, aggregate size, d, decreases with the increase of monoRL surface excess in the aggregates, such that d approaches the stabilized minimum aggregate size (d_{min}) as Γ approaches Γ_{max}. This result indicates that the curvature of the aggregate surface increases with increasing surface excess of monoRL molecules. Because monoRL is anionic and 94% of the monoRL molecules dissociates in PBS, the presence of monoRL causes a negative aggregate surface charge. Enhancement in electrostatic repulsion induces unequal rate of approach for polar and hydrophobic moieties between molecules, and therefore an increase in aggregate surface curvature (Fig. 10). Thus, the aggregate size, d, decreases with increasing Γ. Zeta potential is a function of both particle size and surface charge density.[30, 34, 35] Therefore, it is essentially a function of Γ and its change also exhibits

an asymptotic decrease pattern at concentrations lower than CMC (see Figure 7).

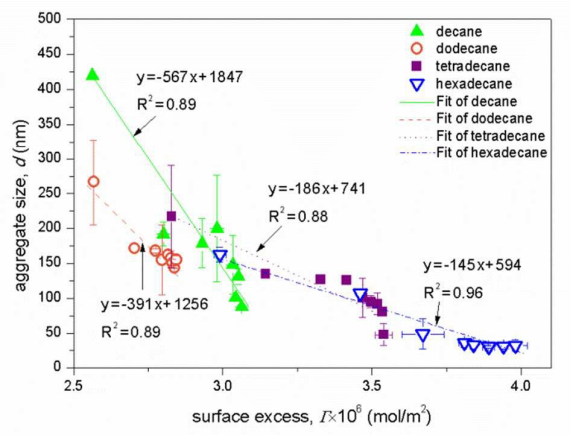

Figure 9 Aggregates diameter (d) versus surface excess of monoRL (Γ) at monoRL bulk concentration (C_w) below CMC. Error bars show mean ± standard deviation.

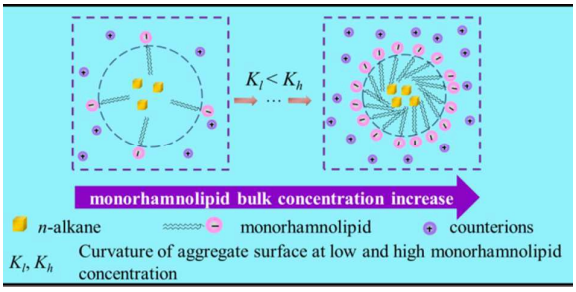

Figure 10 Schematic diagram of alkane-monoRL aggregate formation at monoRL concentration below CMC.

When monoRL concentration in bulk solution (C_w) is higher than CMC, Γ at the aggregate surface reaches Γ_{max} and the size of aggregates reaches the minimum, giving low efficiency for alkane solubilization. As a result, the MSR at monoRL concentrations above CMC is significantly smaller than that for monoRL concentrations below CMC.

5. Conclusion

The results of this study demonstrated that monorRL biosurfactant at concentrations lower than critical micelle concentration can enhance n-alkanes solubilization. The results also support that such solubilization enhancement is caused by an aggregate formation mechanism. Moreover, the solubilization enhancement at sub-CMC concentrations is more significant for the alkanes with chain length similar to monoRL alkyl chain length. This appears to be the first report delineating the mechanism responsible for the sub-critical micelle concentration solubilization of hydrophobic organic compounds by biosurfactant, which successfully explains observations of sub-CMC solubilization of alkanes by rhamnolipid in prior studies (i.e. ref. 8 and 19). The study is of importance for better understanding the solubilization behavior of hydrophobic organic compounds by rhamnolipid and for economical application of rhamnolipid biosurfactant in related areas. Future studies should aim at testing sub-critical micelle concentration solubilization behavior of rhamnolipid for other classes of hydrophobic organic compounds, and in other matrices such as porous media.

Acknowledgments

The authors thank the Center for Integrative Imaging (CII) at University of Science and Technology of China for cryo-TEM analysis. This study was funded by the

National Natural Science Foundation of China (51378192, 51378190, 51308200 and 21276269), and the Program for Changjiang Scholars and Innovative Research Team in University (IRT-13R17). Additional support was provided by the NIEHS Superfund Research Program (P42 ES04940).

References

1 H. Y. Fu, G. M. Zeng, H. Zhong, X. Z. Yuan and G. H. Huang. *Biodegradation*, 2007, **18**, 303-310

2 X. L. Liu, G. M. Zeng, L. Tang, H. Zhong, R. Y. Wang, H. Y. Fu, Z. F. Liu, H. L. Huang and J. C. Zhang. *Process Biochem.*, 2008, **43**, 1300-1303

3 H. Zhong, Y. Liu, Z. F. Liu, Y. B. Jiang, F. Tan, G. M. Zeng, X. Z. Yuan, M. Yan, Q. Y. Niu and Y. S. Liang. *Int. Biodeter. Biodegr.*, 2014, **94**, 152-159

4 I. M. Banat, A. Franzetti, I. Gandolfi, G. Bestetti, M. G. Martinotti, L. Fracchia, T. J. Smyth and R. Marchant. *Appl. Microbiol. Biotechnol.*, 2010, **87**, 427-444.

5 L. M. Abriola, C. D. Drummond, E. J. Hahn, K. F. Hayes, T. C. G. Kibbey, L. D. Lemke, K. D. Pennell, E. A. Petrovskis, C. A. Ramsburg and K. M. Rathfelder, *Environ. Sci. Technol.*, 2005, **39**, 1778-1790.

6 J. Childs, E. Acosta, M. D. Annable, M. C. Brooks, C. G. Enfield, J. H. Harwell, M. Hasegawa, R. C. Knox, P. S. Rao, D. A. Sabatini, B. Shiau, E. Szekeres and A. L. Wood, *J. Contam. Hydrol.*, 2006, **82**, 1-22.

7 D. E. Kile and C. T. Chiou, *Environ. Sci. Technol.*, 1989, **23**, 832-838.

8 Y. Zhang and R. M. Miller, *Appl. Environ. Microb.*, 1992, **58**, 3276-3282.

9 K. D. Pennell, L. M. Abriola and W. J. Weber Jr, *Environ. Sci. Technol.*, 1993, **27**, 2332-2340.

10 J. E. McCray, G. Bai, R. M. Maier and M. L. Brusseau, *J. Contam. Hydrol.*, 2001, **48**, 45-68.

11 J. S. Clifford, M. A. Ioannidis and R. L. Legge, *J. Colloid Interface Sci.*, 2007, **305**, 361-365.

12 J. D. Albino and I. M. Nambi, *J. Environ. Sci. Heal. A*, 2009, **44**, 1565-1573.

13 S. Damrongsiri, C. Tongcumpou, P. Weschayanwiwat and D. A. Sabatini, *J. Hazard. Mater.*, 2010, **181**, 1109-1114.

14 K. Matsuoka, R. Yamashita, M. Ichinose, M. Kondo and T. Yoshimura, *Colloids and Surfaces A: Physicochem. Eng. Aspects*, 2014, **456**, 83-91.

15 A. Patist, J. R. Kanicky, P. K. Shukla and D. O. Shah, *J. Colloid Interface Sci.*, 2002, **245**, 1-15.

16 M. A. Mir, O. A. Chat, M. H. Najar, M. Younis, A. A. Dar and G. M. Rather, *J. Colloid Interface Sci.*, 2011, **364**, 163-169.

17 A. R. Tehrani-Bagha and K. Holmberg, *Materials*, 2013, **6**, 580-608.

18 H. Zhong, L. Yang, G. Zeng, M. L. Brusseau, Y. Wang, Y. Li, Z. Liu, X. Yuan and F. Tan, *RSC Advances*, 2015, **5**, 78142-78149.

19 H. Zhong, Y. Liu, Z. F. Liu, Y. B. Jiang, F. Tan, G. M. Zeng, X. Z. Yuan, M. Yan, Q. Y. Niu and Y. S. Liang, *Int. Biodeter. Biodegr.*, 2014, **94**, 152-159.

20 Y. Ishigami, Y. Gama, H. Nagahora, M. Yamaguchi, H. Nakahara and T. Kamata, *Chem. Lett.*, 1987, **16**, 763-766.

21 L. Chen and T. C. Kibbey, *Langmuir*, 2006, **22**, 6874-6880.

22 S. Peng and M. L. Brusseau, *Water Resour. Res.*, 2005, **41**, 6874-6880.

23 M. J. Rosen, *Surfactants and Interfacial Phenomena*, John Wiley & Sons, Hoboken, 3rd edn., 2004.

24 H. Zhong, Y. Jiang, G. Zeng, Z. Liu, L. Liu, Y. Liu, X. Yang, M. Lai and Y. He, *J. Hazard. Mater.*, 2015, **285**, 383-388.

25 NCBI, PubChem Compound Database; CID=15600, selected properties of n-Decane, http://pubchem.ncbi.nlm.nih.gov/compound/15600, (accessed May 27, 2015).

26 NCBI, PubChem Compound Database; CID=8182, selected properties of n-Dodecane, http://pubchem.ncbi.nlm.nih.gov/compound/8182, (accessed May 27, 2015).

27 NCBI, PubChem Compound Database; CID=12389, selected properties of n-Tetradecane, http://pubchem.ncbi.nlm.nih.gov/compound/12389, (accessed May 27, 2015).

28 NCBI, PubChem Compound Database; CID=11006, selected properties of n-Hexadecane, http://pubchem.ncbi.nlm.nih.gov/compound/11006, (accessed May 8, 2015).

29 X. Z. Yuan, F. Y. Ren, G. M. Zeng, H. Zhong, H. Y. Fu, J. Liu and X. M. Xu, *Appl.*

Microbiol. Biot., 2007, **76**, 1189-1198.

30 R. J. Zasoski, in *Encyclopedia of Soil Science*, ed. W. Chesworth, Springer Netherlands, Dordrecht, 2008, pp. 841-845.

31 H. Zhong, G. M. Zeng, J. X. Liu, X. M. Xu, X. Z. Yuan, H. Y. Fu, G. H. Huang, Z. F. Liu and Y. Ding, *Appl. Microbiol. Biot.*, 2008, **79**, 671-677.

32 D. A. Edwards, R. G. Luthy and Z. Liu, *Environ. Sci. Technol.*, 1991, **25**, 127-133.

33 W. Liu, J. Kumar, S. Tripathy and L. A. Samuelson, *Langmuir*, 2002, **18**, 9696-9704.

34 D. A. Dzombak and F. M. M. Morel, *Surface Complex Modeling,Hydrous Ferric Oxide*, John Wiley & Sons, New York, 1990.

35 R. J. Hunter, *Zeta Potential in Colloid Science. Principles and Applications*, Academic Press, New York, 1981.

Table of contents entry

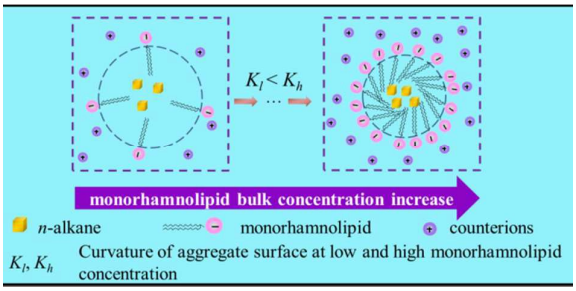

Monorhamnolipid biosurfactant at concentrations lower than CMC enhances *n*-alkanes solubilization due to aggregate formation mechanism. The sub-CMC aggregate size decreases with increasing surface excess of monorhamnolipid.